Development and Evaluation of Active/Lighting Marker in Turbidity and Illumination Variation Environments

1st Yoshiki KANDA
Graduation school of Natural Science and Technology, Okayama University
Okayama, Japan
pw1w867s@s.okayama-u.ac.jp

2nd Naoki MUKADA
Graduation school of Natural Science and Technology, Okayama University
Okayama, Japan
pola9zud@s.okayama-u.ac.jp

3rd Daiki YAMADA
Graduation school of Natural Science and Technology, Okayama University
Okayama, Japan
p7kw2h27@s.okayama-u.ac.jp

4th Khin LWIN
Graduation school of Natural Science and Technology, Okayama University
Okayama, Japan
pdoj8yez@s.okayama-u.ac.jp

5th Myo MYINT
Graduation school of Natural Science and Technology, Okayama University
Okayama, Japan
puqs1ci8@s.okayama-u.ac.jp

6th Kohei YAMASHITA
Graduation school of Natural Science and Technology, Okayama University
Okayama, Japan
p9mk0tyb@s.okayama-u.ac.jp

7th Sho NAKAMURA
Graduation school of Natural Science and Technology, Okayama University
Okayama, Japan
pc7y9wqz@s.okayama-u.ac.jp

8th Takayuki MATSUNO
Graduation school of Natural Science and Technology, Okayama University
Okayama, Japan
matsuno@cc.okayama-u.ac.jp

9th Mamoru MINAMI
Graduation school of Natural Science and Technology, Okayama University
Okayama, Japan
minami-m@cc.okayama-u.ac.jp

***Abstract*—To extend the persistence time of an underwater operation of AUVs in the sea, many studies have been performed worldwide. The docking function takes place as an important role not only for battery recharging but also for other advanced applications. Therefore, we developed the visual-servoing-based underwater vehicle using 3D perception based move on sensing (3D-MoS) system with dual-eye cameras and 3D marker for the docking operation. The vision-based underwater vehicle cannot avoid the turbidity and low illumination in the deep sea. In the present study, the active/lighting marker was newly designed and constructed to improve the recognizing ability of the proposed system for the real-time 3D pose estimation. The experiments were conducted in a simulated pool against different turbidity levels and illumination variations by adjusting the LED's brightness of the active marker in both day and night environments. This paper presents the analyses on the relations of the currents of LED installed inside each ball of the 3D marker and recognition results under turbidity and changing illumination conditions. According to the experimental results, the optimum current was chosen for the docking.**

***Index Terms*—Pose estimation, Turbidity, Illumination variation, Active/Lighting 3D marker, LED's current**

I. Introduction

Japan has wide areas of the sea from which natural resources can be taken out using advanced technologies. Autonomous Underwater Vehicle (AUV) has been expected to play important roles in a deep sea such as oil pipe inspection, the survey of seafloor, searching rare metal, etc. Methane hydrate could be a future energy solution. To realize such tasks that take long period in the deep sea, one of the main hinders of AUVs is limited power capacity. To solve this problem, underwater battery recharging with a docking to the charging station is one of the solutions to extend the operation time of AUVs.

Most of the studies related to vision based navigation for underwater vehicle are based on single camera[1][2]. Apart from them, we have been studying a stereo-vision based docking approach for AUV. In our approach, the relative pose between the underwater vehicle and a 3D marker is estimated using Real-time Multi-step GA (RM-GA) that is real-time 3D pose estimation method. Avoiding the disadvantages of dual-eyes 3D perception by features based recognition methods that has been researched and are based on 2D-to-3D reconstruction, 3D model based matching method that is based on 3D-to-2D projection method is used in our approach. One of the main drawbacks of 2D-to-3D reconstruction is that incorrect mapping between corresponding points in images, resulting in erroneous pose estimation.

Since the underwater environment is complex, there are many disturbances for vision-based underwater vehicles. Therefore, it is important to devise how to overcome the possible disturbances before testing in the sea. The common disturbances for the vision-based underwater vehicle are light environment changing and turbidity. Since underwater battery recharging units are supposed to be installed at the sea

978-1-5386-1654-3/18/$31.00 ©2018 IEEE

bottom, the deep sea docking experiments cannot avoid the turbidity and low light environment. As far as the authors have researched, there is no practical system for recharging with performances of tolerance against illumination and turbidity varieties. In our previous works [3]-[7], the 3D pose estimation and the docking operation were conducted by using the passive marker and the Remotely Operation Vehicle (ROV) in clear water environment. However, the recognition accuracy using the passive marker and ROV's LED is limited to lower turbidity environment. To expand recognition tolerance against turbidity and illumination, an active 3D marker has been designed and constructed. The difference between the passive marker and the active marker is that the LEDs were installed inside the three balls of the marker, and the former not. The recognizing ability in turbidity environment can be improved by making the marker emit instead of ROV's LED lighting source for a passive marker. However, the recognition accuracy changes depending on the LED's brightness of the active marker due to the reduction of color information of the 3D marker when the lower or higher currents of LED are given. Recognition experiments to find the relations of currents of LED and recognition results under different light and turbidity levels have been conducted to decide appropriate LED's current. We aim to construct the system which adapts all environments.

This paper is organized as follows: Section Ⅱ discusses 3D move on sensing using Real-time Multi-step GA. Section Ⅲ describes the experiments, results and discussion. Conclusion and areas of future work are presented in section IV.

II. 3D Move on Sensing (3D-MoS) using Real-Time Multi-Step GA

The 3D-MoS system that uses three dimensional measurement with solid object recognition based on visual servoing technology was already introduced and explained in [8]. In this system, model-based matching method is used to estimate the relative pose between the vehicle and a known 3D marker. Here, 3D pose estimation using RM-GA briefly for the background of readers is discussed in this section. Figure 1 shows the model-based matching method using dual-eye cameras for 3D pose estimation. In Fig. 1, Σ_{CL} and Σ_{CR} are the reference coordinate frames of the right camera and the left camera. Σ_H is the reference frame of the ROV. Σ_M is the reference frame of the real target object. Σ_{M_i} is the reference frame of the i-th model. The real target object in 3D search space is projected naturally to the dual-eyes cameras images and the dotted 3D marker model, where the pose is given by one of GA's genes, is projected from 3D-to-2D. The correlation function of each projected model is evaluated by designed fitness function. Finally, the best model of the target object that represents the true pose can be obtained based on its highest fitness value. Equation 1 shows the fitness function. The fitness function is constructed and designed to evaluate the matching degree between the projected models and the captured images. The fitness function has maximum value when the model and the real target exactly coincide. The true pose of the target object is expressed with the peak of the mountain shape in the fitness distribution. Detailed explanation of the fitness function is referred to our previous paper [9].

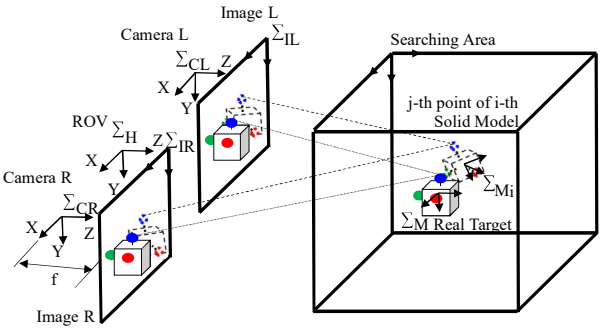

Fig. 1. Model-based matching method using dual-eye cameras and 3D marker. A solid object in 3D space is the real target and dotted ones in 3D and 2D space are models. The correlation function of each projected model is evaluated by designed fitness function.

$$
\begin{aligned}
F(\boldsymbol{\phi}_i) = \Bigg\{ & \Bigg(\sum_{{}^{IL}\boldsymbol{r}_i(\boldsymbol{\phi}_i) \in S_{L,in}(\boldsymbol{\phi}_i)} p({}^{IL}\boldsymbol{r}_i(\boldsymbol{\phi}_i)) \\
& - \sum_{{}^{IL}\boldsymbol{r}_i(\boldsymbol{\phi}_i) \in S_{L,out}(\boldsymbol{\phi}_i)} p({}^{IL}\boldsymbol{r}_i(\boldsymbol{\phi}_i)) \Bigg) / N \\
& + \Bigg(\sum_{{}^{IR}\boldsymbol{r}_i(\boldsymbol{\phi}_i) \in S_{R,in}(\boldsymbol{\phi}_i)} p({}^{IR}\boldsymbol{r}_i(\boldsymbol{\phi}_i)) \\
& - \sum_{{}^{IR}\boldsymbol{r}_i(\boldsymbol{\phi}_i) \in S_{R,out}(\boldsymbol{\phi}_i)} p({}^{IR}\boldsymbol{r}_i(\boldsymbol{\phi}_i)) \Bigg) / N \Bigg\} / 2 \\
= & \{F_R(\boldsymbol{\phi}_i) + F_L(\boldsymbol{\phi}_i)\} / 2
\end{aligned} \tag{1}
$$

A. Real-time Multi-step GA

In the proposed 3D model-based recognition method, searching for all possible models is time consuming for real-time recognition. Therefore, the problem of finding/recognizing the 3D marker and detecting its pose is converted into an optimization problem with a multi-peak distribution. The genetic algorithm is selected and utilized as RM-GA to search the best solution within 33[ms]. Figure. 2 shows the flowchart of the RM-GA. Position and orientation of the three-dimensional model are represented as an individual of the chromosome that is 72 bit string in RM-GA. The former 36 bits represent the position of the 3D marker and the later 36 bits describe the orientation defined by a quaternion. Firstly, a random population of the chromosome is generated. A new pair of left and right images is input. The RM-GA procedure is performed within 33 [ms]. The RM-GA finds repeatedly the solutions to get the best pose of the target object within the video frame rate to deal with time varying distribution for newly input images. Finally, the best pose of the individual represents the true pose of the real target. Although the pose

of the target object is evaluated in 2D, convergence occurs in 3D. For the next input, a new video image is used.

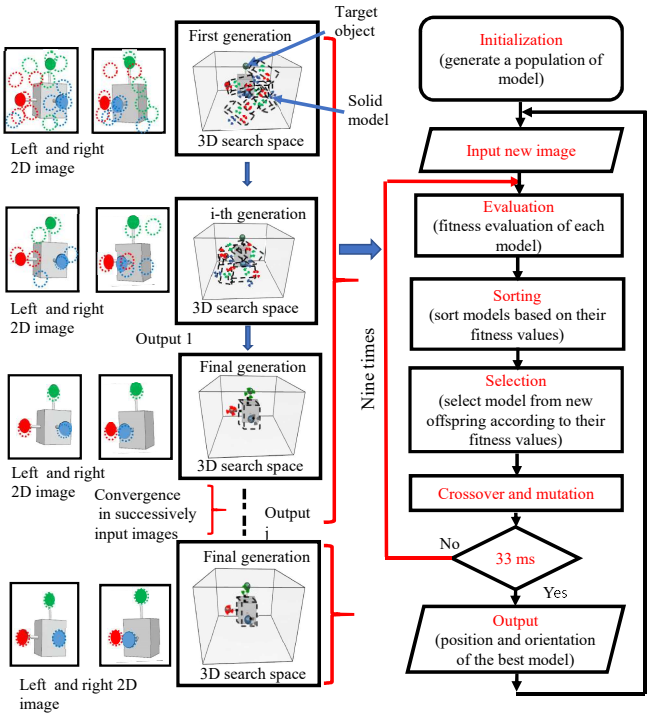

Fig. 2. Flowchart of the real-time multi-step GA

B. Remotely Operated Vehicle

Hovering type underwater vehicle (manufactured by Kowa cooperation) was used as a test bed as shown in Fig. 3. Two fixed cameras installed at the front of the vehicle are used as the main sensor. In thruster unit, four thrusters are controlled with maximum thrust force of 4.9 [N]. The vehicle can dive in maximum water depth 50 [m] and two LED light sources are also installed on the vehicle.

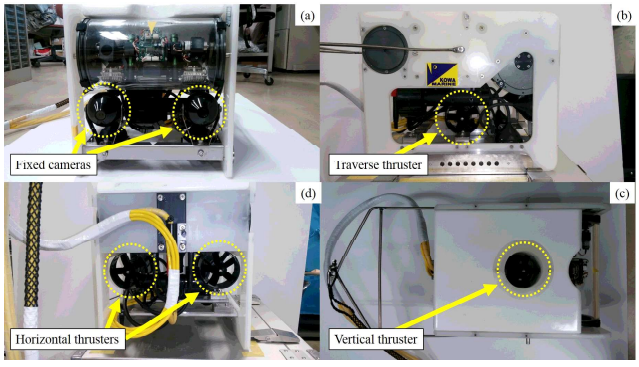

Fig. 3. Photograph of ROV (a) Front view showing two cameras, (b) Side view showing traverse thruster, (c) Back view showing horizontal thrusters, and (d) Top view showing vertical thruster.

C. Active/Lighting 3D marker

In our previous works [1]-[5], we conducted the experiments using the passive marker. In the present study, the 3D pose estimation system was improved by constructing the active marker that can emit the light. Figure 4 shows the appearance of the active marker. The difference between the passive marker and the active marker is that the LEDs were installed inside the three balls of the marker. The 3D marker is constructed from a water proof box (100 [mm] $\times$ 100 [mm] $\times$ 100 [mm]) and the white spheres (diameter: 40 [mm]) are attached to the water proof box. The red, green and blue LED were installed into the white spherical ball that is covered by the color balloon. The internal circuit diagram of the active marker is shown in Fig. 5. The red, green, and blue LEDs were used and each current of LED was adjusted by using variable resisters.

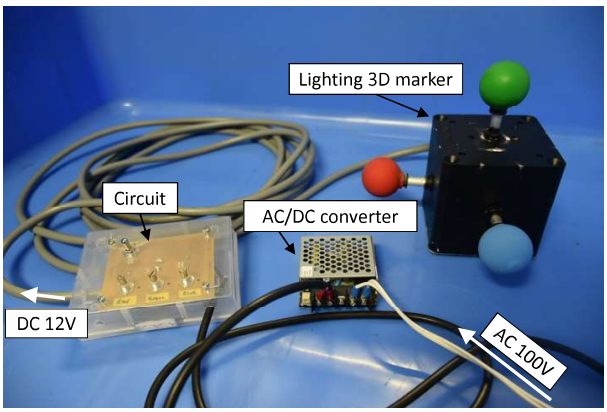

Fig. 4. Active/Lighting 3D marker

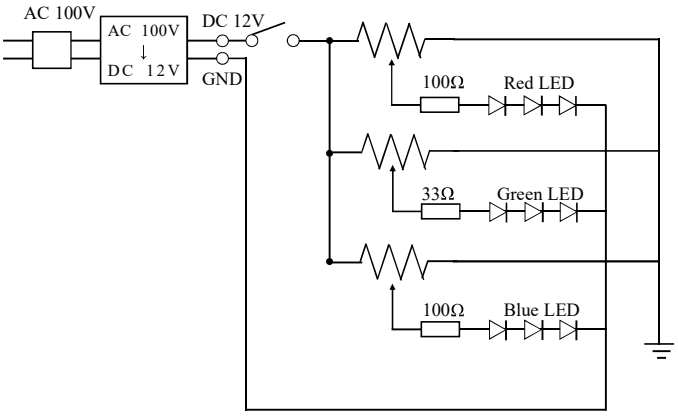

Fig. 5. Internal circuit diagram of the active marker.

III. Experiments, Results and Discussion

A. Turbidity and Illumination

Turbidity (Formazin Turbidity Unit, FTU) is defined as the degree of water muddiness. The turbidity level was measured

by using a portable turbidity sensor (model: TD-M500 manufactured by OPTEX) as shown in Fig. 6(A). Figure 7 shows the appearance of the left and right camera images under different turbidity levels ((A) 0 [FTU], (B) 8 [FTU]). Illumination (lux, lx) is defined as the degree of lighting power and it was measured by using a portable waterproof lux meter (model: MW-700 manufactured by Milwaukee) as shown in Fig. 6(B). Figure 8 shows the appearance of the left and right camera images under different illumination conditions ((A) 1400 [lx], (B) 200 [lx]).

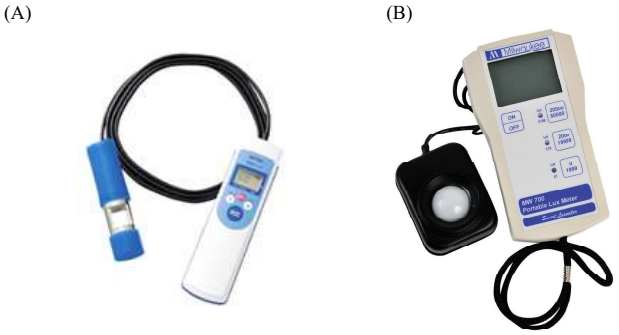

Fig. 6. Measuring instrument : (A) Portable turbidity sensor TD-M500, (B) Portable waterproof lux meter MW-700

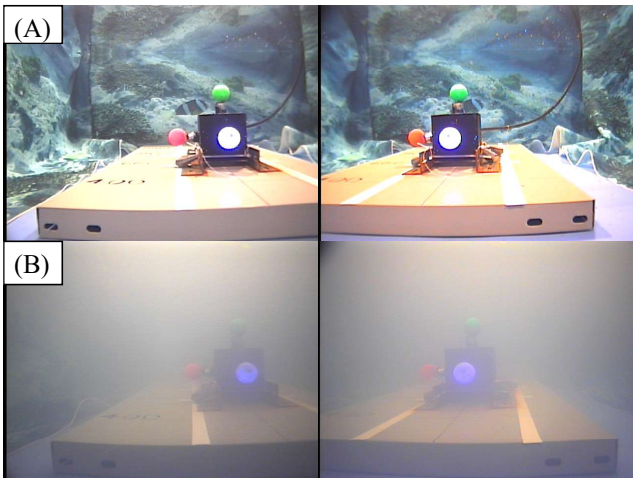

Fig. 7. The appearance of left and right camera images at different turbidity levels under the same illumination and current of LED inside the active marker: (A) 0 [FTU], (B) 8 [FTU].

B. Experimental layout

The 3D pose estimation experiment was conducted in the simulated pool by changing illumination in different turbidity levels. Figures 9 and 10 show the experimental layout and coordinate system of the ROV. In this experiment, the ROV and the active marker were fixed in position at the distance 600 [mm]. The amount of turbidity was controlled from 0 to 12 [FTU] by adding milk in water in the tank. Milk was

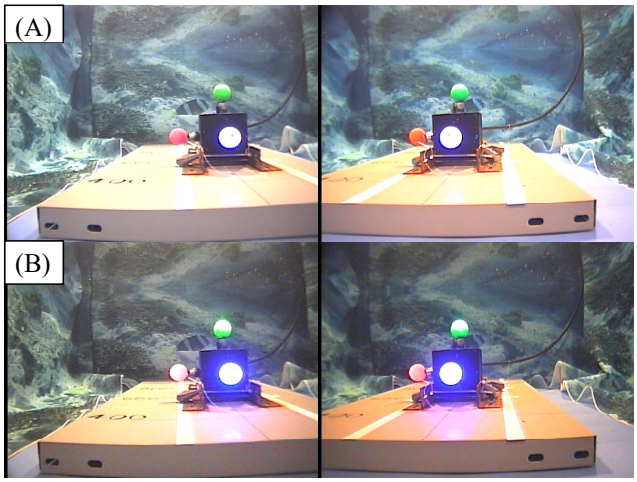

Fig. 8. The appearance of left and right camera images at different illuminations under the same turbidity levels and current of LED inside the active marker: (A) 1400 [lx] (B) 200 [lx].

selected to simulate the turbidity because it can provide all types of scattering [10][11]. The illumination was simulated from 0 to 1400 [lx] in each turbidity level by controlling four lighting sources that are placed at the four corners of the pool as shown in Fig. 9.

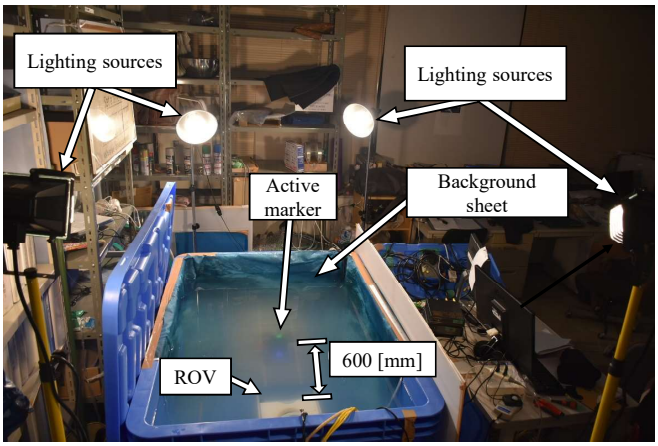

Fig. 9. Experiment environment with simulated lighting and turbidity

C. 3D pose estimation experiment

The results of the experiment are shown in Figs. 11-13. The brightness of the LED of the active marker was increased from 0 [mA] to 16 [mA] with difference 2 [mA] for changing illumination conditions from 0 [lx] to 1400 [lx] with difference 200 [lx] for each turbidity level. The experiment was conducted in the cases of four turbidity levels such as 0 [FTU], 4 [FTU], 8 [FTU], and 12 [FTU], respectively. Figure 11(A)-(D) show the mean fitness values of each current of LED inside active marker by changing illumination conditions in each turbidity level. The vertical axis is fitness value and the horizontal axis

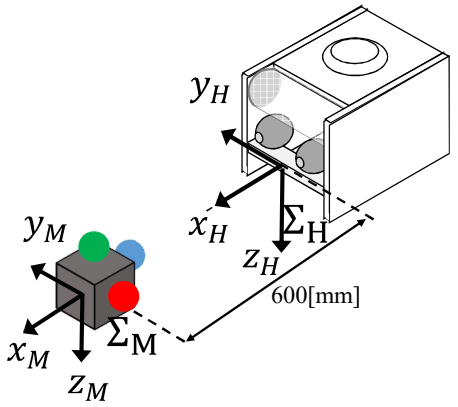

Fig. 10. Coordinate system of ROV and 3D marker

is described by illumination in [lx]. The mean fitness value was calculated in 60 [s]. According to the graphical results, the fitness value of each current of LED gradually decreased from above 1 to about 0.2 when the turbidity was increased under the different illuminations. Figure 12 shows the average fitness value and standard deviation of each current of LED in turbid water. The vertical axis is fitness value and horizontal axis is current in [mA]. It can be concluded that the fitness values for the current value 2 [mA], 4 [mA], and 6 [mA] were above 0.7 in the case of 0 [FTU] and 4 [FTU]. In 8 [FTU], the fitness value was above 0.4. When the turbidity increased to 12 [FTU], the fitness was above 0.3 in the case of 2 [mA], 4 [mA], and 6 [mA]. Three current values 2 [mA], 4 [mA] and 6 [mA] were choose as the appropriate once because the average fitness value is higher and standard deviation is lower than the others. To confirm the best current among these three current values, we checked the fitness distribution by using full search method and hue distribution in 8 [FTU] under dark environment (0 [lx]). The environmental condition of 8 [FTU] and 0 [lx] was considered based on the conditions of previous experiments in the sea.

The full search is a method in which the result of real-time multi-step GA was evaluated by analysing the left and right images where real-time multi-step GA gets the corresponding fitness value. The main idea of full search is to calculate the fitness of every points which are 1 [mm] apart in the entire searching area. The fitness distribution and the hue distribution against turbidity under dark environment in the case of 6 [mA], 4 [mA], and 2 [mA] are shown in Fig. 13 (I), (II), and (III). The first row of Fig. 13 I(a) shows the fitness value distribution in x-y plane by 3D graph where the position in z-direction and orientation were fixed in the full search method. The peak of the mountain shape represent the true pose of the target. The 2D graph of fitness distribution is shown in Fig. 13 I(b). The intersection shape of "X" type can be seen in x-y plane, and the distribution peak appears at the intersection point as shown in 2D graph. Fig. 13 I(c) shows the left and right camera images and hue distribution in the case of 6 [mA]. Figures 13 (II) and (III) show the result of 4 [mA], and 2 [mA] respectively. In fitness value distribution, it can be seen that the highest peak occurs in the case of 4 [mA] with the maximum fitness value F_{max} 0.87. In hue distribution, the hue value of blue ball is out of hue range that is defined in the experiment, therefore, the proposed system did not recognize the blue ball in the case of 6 [mA]. At 4 [mA] and 2 [mA], the hue values of all balls exist in the hue range of each color. According to the experimental results, 4 [mA] is the best current for each LED against turbidity and illumination.

IV. Conclusion

In the present paper, checking the relationship between turbidity, illumination and current of LEDs installed in active 3D marker and choosing appropriate current of LEDs was proposed. The results of 3D pose estimation experiment against turbidity under day and night environment in the simulated pool were presented. According to the experimental results, 4 [mA] is appropriate LED's current. The docking experiments will be conducted in the real sea with turbid environments using this LED's current.

Acknowledgment

The authors would like to thank Monbukagakusyo; and Kowa Corporation for their collaboration and support for this study.

References

[1] Feezor M D, Sorrell F Y, Blankinship P R, "Bellingham J G(2001) Autonomous underwater vehicle homing/docking via electromagnetic guidance", IEEE Journal of Oceanic Engineering, 26(4):515-521

[2] Negre A, Pradalier C, "Dunbabin M(2008) Robust vision-based underwater homing using self-similar landmarks", Journal of Field Robotics, 25(6-7):360-377

[3] Myint, M., Yonemori, K., Yanou, A., Ishiyama, S., Minami, M., "Robustness of visual-servo against air bubble disturbance of underwater vehicle system using three-dimensional marker and dual-eye cameras", In OCEANS 2015-MTS/IEEE, Washington DC, USA (2015), pp. 1-8.

[4] Myint, M., Yonemori, K., Yanou, A., Lwin, K.N., Minami, M., Ishiyama, S., "Visual servoing for underwater vehicle using dual-eyes evolutionary real-time pose tracking", Journal of Robotics and Mechatronics,28(4), pp.543-558, 2016.

[5] Myint, M., Yonemori, K., Yanou, A., Lwin, K N., Minami, M., Ishiyama, S., "Visual-based deep sea docking simulation of underwater vehicle using dual-eyes cameras with lighting adaptation", Proceedings of OCEAN 2016-Shanghai, (2016), pp. 1-8.

[6] Myint, M., Yonemori, K., Yanou, A., Lwin, K N., Mukada, N., Minami, M., "Dual-eyes visual-based sea docking for sea Bottom battery recharging", OCEAN (2016).

[7] Xiang Li, Yuya Nishida, Myo Myint, Kenta Yonemori, Naoki Mukada, Khin Nwe Lwin, Matsuno Takayuki, Mamoru Minami, "Dual-eyes Vision-based Docking Experiment of AUV for Sea Bottom Battery Recharging", MTS / IEEE OCEANS '17, Aberdeen Scotland, June 19-22, 2017.

[8] Myo Myint, Kenta Yonemori, Khin Nwe Lwin, Akira Yanou, Mamoru Minami. JIntell Robot Syst (2017). DOI 10.1007/s10846-017-0703-6.

[9] Song, W.,Minami, M., Aoyagi, S., "On-line stable evolutionary recognition based on unit quaternion representation by motion-feedforward compensation", International Journal of Intelligent Computing in Medical Science and Image Processing, 2(2), pp.127-139, 2008.

[10] Garcia, R. and Gracias, N., "Detection of interest points in turbid under water", OCEANS, 2011 IEEE-Spain, pp.1-9, 2011.

[11] Condevilla, F,. Gaya, J.D.O., Duarte, N. and Botelho, S., "Achieving turbidity robustness on underwater images local feature detection", International journal of computer vision, 60(2), pp.91-110, 2004.

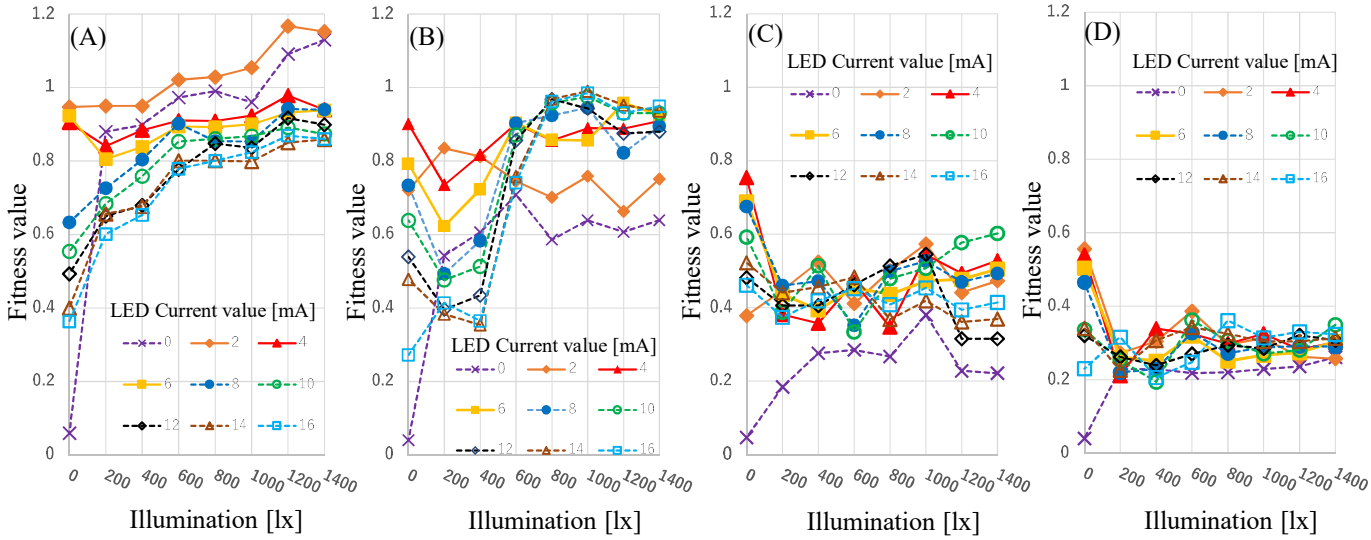

Fig. 11. The mean fitness value of each current of LED inside the active marker under different illuminations and turbidity levels : (A) 0 [FTU], (B) 4 [FTU], (C) 8 [FTU], (D) 12 [FTU].

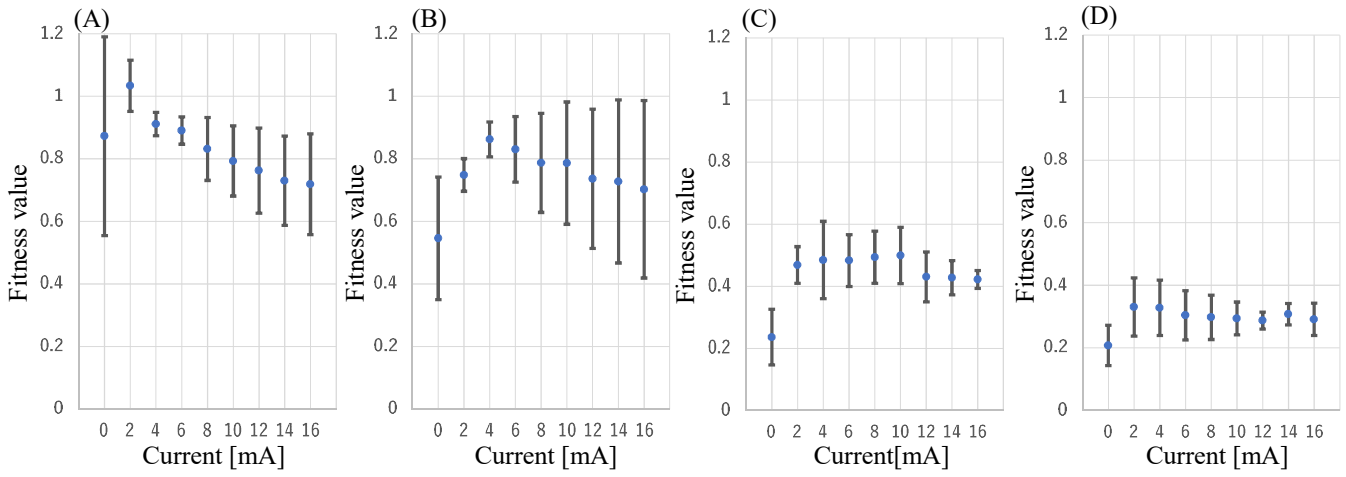

Fig. 12. Average fitness value and standard deviation of each current of LED inside the active marker under different turbidity levels : (A) 0 [FTU], (B) 4 [FTU], (C) 8 [FTU], (D) 12 [FTU]. The corresponding numerical data are shown in Fig. 11.

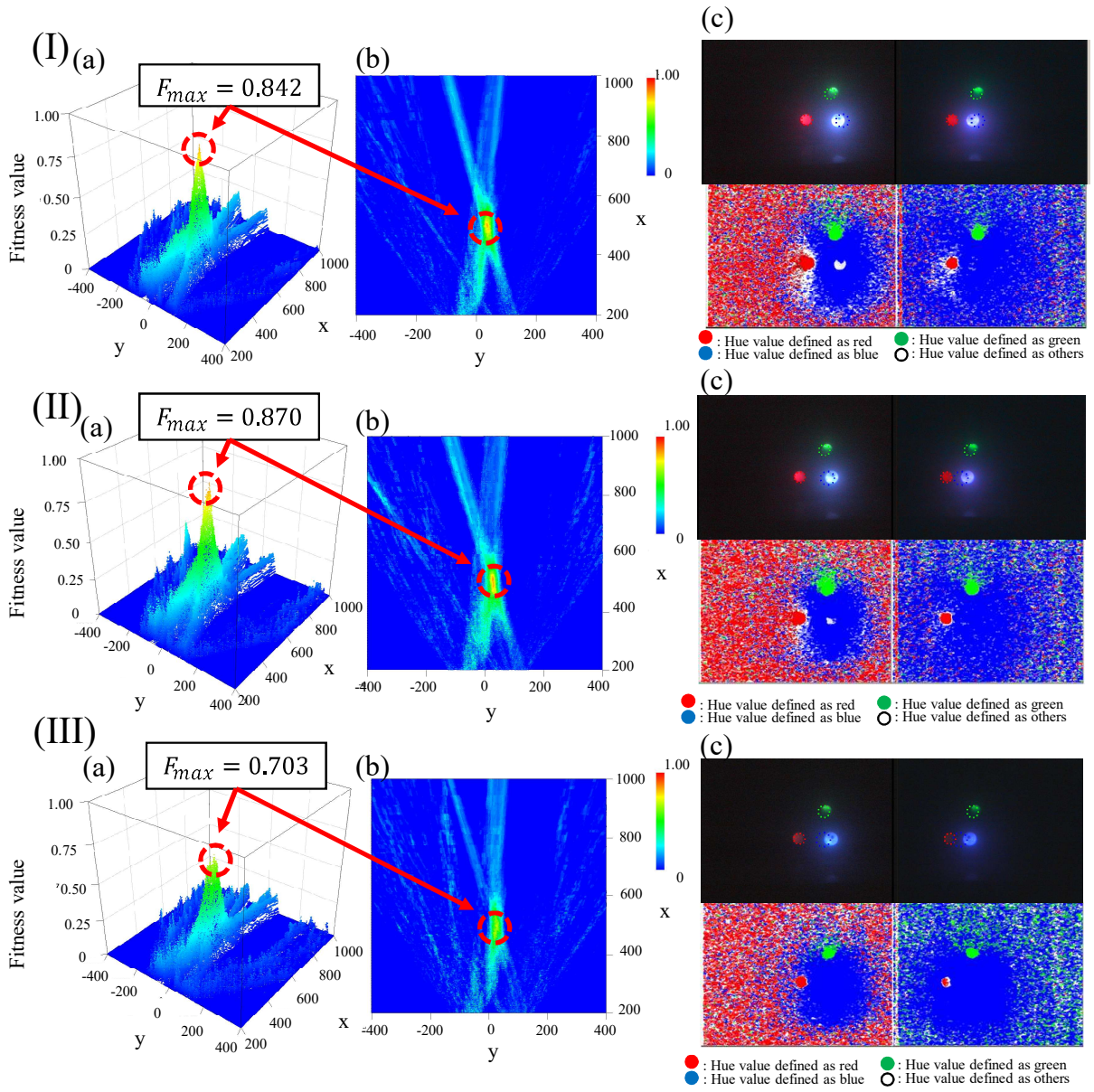

Fig. 13. Fitness value distributions in fixed position in z-direction and orientation, left and right camera images and hue distributions under different LED's current of the active marker((I) 6 [mA], (II) 4 [mA], (III) 2 [mA]) in 8 [FTU] and 0 [lx] at the distance 600 [mm] between the ROV and 3D marker. Fitness value distributions are shown by 3D graph as shown in Fig. 13 (a), and 2D graph as shown in Fig. 13 (b). F_{max} is the highest fitness value in each fitness value distribution. Hue distributions of left and right camera images are shown in Fig. 13 (c). In hue distributions, red, green, blue and white dots are defined as hue value of red, green, blue and others in our system.